Molecular Vision 2024; 30:305-318 <http://www.molvis.org/molvis/v30/305>
Received 27 March 2023 | Accepted 2 October 2024 | Published 4 October 2024

Genetic implications of CHST6 gene mutations and their corneal microstructural changes in macular corneal dystrophy patients

Durga Murugan,[1] Roopam Duvesh,[1] Sindhura Devi Adsumilli,[2] Namperumalsamy Venkatesh Prajna,[2] Prakash Chermakani,[1,3] Periasamy Sundaresan[1]

(The first two authors contributed equally to this work)

[1]Department of Genetics, Aravind Medical Research Foundation, Madurai, Tamil Nadu, India; [2]Cornea Clinic, Aravind Eye Hospital, Madurai, Tamil Nadu, India; [3]Department of Molecular Biology, Aravind Medical Research Foundation - Affiliated to Alagappa University, Karaikudi, Tamil Nadu, India

Purpose: To collectively investigate the carbohydrate sulfotransferase 6 (CHST6) mutation spectrum and corneal morphological alterations of macular corneal dystrophy (MCD) patients using in vivo confocal microscopy (IVCM), histochemistry, immunohistochemistry, and further ascertaining the immunophenotype using an enzyme-linked immunosorbent assay (ELISA).

Methods: Sanger sequencing-based CHST6 gene screening was performed for 112 study participants (MCD patients, n = 68; family members, n = 44). Twenty-seven MCD patients underwent IVCM analyses, and corneal buttons were analyzed with histochemistry Alcian blue (AB) staining and immunohistochemistry anti-keratan sulfate (KS) monoclonal antibody, 5D4MoAb. An ELISA was used to determine serum KS levels. Quantitative analysis of the central corneal thickness (CCT), epithelial cell thickness, epithelial cell count, and stromal keratocyte cell count was performed using a one-way ANOVA.

Results: Eighteen distinct CHST6 mutations, including one novel (p.L129V), were identified. MCD patients with predominant immunophenotype IA (n = 15) harboring major p.Q182Rfs199 deletion, p.194_R196delinsRC (delins), and open reading frame (ORF) mutations displayed AB positivity corresponding to loss of Bowman's layer, interlamellar glycosaminoglycan (GAG) depositions, and faint KS expression (5D4-MoAb) only in stromal keratocytes. Notably, IVCM imaging revealed BL loss due to confluent clumps of hyper-reflective, granular deposits together with scar tissue seen only in this group. Eight patients (with missense mutations) displayed immunophenotype I with positive GAG deposits and negative KS expression. Patients with immunophenotype II (n = 4) with no mutations showed both positive GAG deposits and KS expression. A quantitative analysis revealed a statistically significant decrease in CCT (p-value < 0.001), epithelial cell thickness, epithelial cell count, and stromal keratocyte cell count among the patients with truncation mutations compared to the control group.

Conclusions: In this current study, the combinational findings of MCD-related corneal morphological alterations, immunophenotypes, and mutation spectrum are presented first, which indicated a severe phenotype in patients identified with truncation (deletion, delins, and deletion of ORF) mutations. However, additional studies with a larger number of patients would help highlight these findings and reinforce the possible correlation between genotypes and immunophenotypes in MCD pathogenesis.

Macular corneal dystrophy (MCD; OMIM 217800) is a rare but severe corneal dystrophy that primarily affects the stroma, although the involvement of other corneal layers has also been reported. Characteristic manifestations of MCD include the presence of punctate gray-white opacities beneath the epithelium, stroma, Descemet's membrane, and corneal endothelium [1]. The presence of abnormal deposits results in a central hazy stroma, which also gradually extends to the peripheral cornea. Typically observed with early onset, and owing to its progressive nature, MCD results in the involvement of the full-length stroma until the limbus with bilateral dense clouding of the cornea by the second decade of life, thus eventually affecting a patient's vision severely by their second or third decades and often necessitating penetrating keratoplasty (PKP) [2].

MCD is an autosomal recessive disease with a reported higher frequency in Southern India, Saudi Arabia, and Iceland, ascribed to the large pool of candidate carbohydrate sulfotransferase 6 (CHST6) gene mutations underlying MCD pathology. Notably, the higher prevalence of MCD in South Indian and Saudi Arabian populations is attributed to the practice of consanguineous marriage [3,4]. The CHST6 gene on the short arm of chromosome 16 (16q23.1) encodes a 395 amino acid protein, which is a corneal enzyme

Correspondence to: Periasamy Sundaresan, Department of Genetics, Aravind Medical Research Foundation, 1, Anna Nagar, Madurai −625020, Tamil Nadu, India. Phone: +91-452-435 6100 (Extn: 423), email: sundar@aravind.org

N-acetylglucosamine-6-O-sulfotransferase (C-GlcNAc6ST) that mediates the sulfation of keratan chains on the core protein of the proteoglycan complex, thus producing sulfated keratan sulfate (KS)—a glycosaminoglycan (GAG). CHST6 mutations affect enzyme activity, leading to the formation of an unsulfated or partial-sulfated form of KS [5], thus resulting in the abnormal accumulation of GAG deposits across corneal layers. These GAG deposits in the form of opacities and clouding ultimately impact corneal transparency and visual acuity [6]. As MCD involves deposit aggregation, in an earlier study, the role of the ubiquitin/proteasomal protein degradation pathway in MCD pathogenesis was studied, which suggested impaired proteasomal clearance [7].

Three immunophenotype variants (MCD types I, IA, and II) have been identified for MCD based on the immunoreactivity of antigenic keratan sulfate (AgKS; sulfated epitopes) to anti-KS antibodies in the cornea and serum, although these immunophenotypes are not clinically distinguishable [4,8]. In Type I, sulfated KS is not detectable (no AgKS reactivity) in both cornea and serum, whereas in Type II, reference or normal KS levels are present in serum, and corneal tissue has AgKS expression. The third type, IA, was initially detected in Saudi MCD patients and then in German patients [4,9]. In MCD Type IA, the patients' serum showed the absence of KS, but stromal keratocytes displayed immunoreactivity to KS antibodies.

Although histopathological investigations are standard practices for detecting corneal dystrophy in clinical settings, advancements in imaging modalities, including in vivo confocal microscopy (IVCM), allow us to visualize the detailed cellular microstructure deep in vivo across the different corneal layers [10]. It offers a noninvasive way to assess the morphology in normal subjects and even in several disease conditions, such as MCD, Fuchs endothelial corneal dystrophy, and other corneal dystrophies, to compare and confirm the diagnosis in less time.

Individual studies have been undertaken to understand MCD disease in various aspects, including mutational screening, histochemistry, immunohistochemistry, in vivo confocal analysis, and KS expression in sections and serum. Nevertheless, earlier studies were either performed on a few samples or not studied in different aspects at a time on the same patients. Herein, a comprehensive combinatorial study was conducted to identify correlations among Indian MCD patients, including identification of mutations, associated corneal morphological changes, structural changes, corneal KS expression based upon histochemistry, immunohistochemistry, in vivo confocal microscopy studies, and serum KS concentration, using an ELISA method.

METHODS

Ethics statement: The study protocols conformed to the tenets of the Declaration of Helsinki and were approved by the Institutional Ethics Committee of Aravind Eye Hospital (AEH), Madurai, Tamil Nadu, India. Written informed consent was obtained from all the study patients and available family members or guardians in the case of minor participants.

Study participants and sample details: This study included 68 individuals of Indian descent presenting with distinct manifestations of the MCD phenotype diagnosed at the cornea clinic of the Aravind Eye Care System in Madurai. Additionally, 44 family members were included in this study. Patients who displayed concurrent findings of MCD with other corneal dystrophies (such as congenital stromal corneal dystrophy, Fleck corneal dystrophy, and posterior amorphous corneal dystrophy) were excluded from this study. Approximately 5 ml of peripheral blood samples were collected in EDTA-vacutainer tubes from 112 study participants (68 MCD patients and 44 family members), and genomic DNA was isolated using a modified salt precipitation method for genetic analysis (explained in a later section) [11]. Also, 150 age- and ethnic-matched individuals without any history of ocular or corneal diseases were included as controls for the analysis.

Furthermore, IVCM analysis was performed on 25 MCD patients and two affected family members before penetrating keratoplasty (PKP). Following PKP, corneal buttons were collected for corneal morphology analysis and KS distribution using the histochemistry (HC) and immunohistochemistry (IHC) methods. Also, corneal tissues were excised from 10 age-matched human cadaver eye globes (donor age > 10 years) that were enucleated within 6 hours of death, followed by the preservation of these buttons in McCarty-Kaufman medium and received for research work within 24 hours. These cadaver globes (non-optical grade) were obtained from the Rotary Aravind International Eye Bank at AEH (Madurai) without any history of ocular or systemic disease. KS levels were quantified in serum samples from the same patients (n = 27), along with 50 healthy individuals as controls.

Ocular assessments: Comprehensive ophthalmic examinations, including visual acuity and slit-lamp biomicroscopy (SLM-3X-Slit-Lamp, China), were performed on all the study patients. Additional documented details included a detailed medical or family history of MCD, symmetry, pedigree, and age at presentation or onset. The diagnosed MCD patients showed evidence of fine, superficial, and grayish-white punctate opacities, especially in the superficial cornea, giving them a dense, cloudy appearance. Macular spots with indistinct edges were observed, with unclear intervening stroma.

In vivo confocal microscopy: Corneal IVCM analysis was performed using the Heidelberg Retina Tomograph3 (HRT3) with the Rostock Corneal Module (RCM; Heidelberg Engineering GmbH, Heidelberg, Germany) after the instillation of an anesthetic 0.5% proparacaine eyedrop (Aurocaine, Aurolab, Madurai, India). Due to the direct applanation of the corneal surface to HRT3 RCM (with a water immersion objective of 63x), a sterile single-use TomoCap (Heidelberg Engineering, Heidelberg, Germany) was used, coupled with GenTeal gel (Novartis India Limited, Mumbai) with a refractive index like that of the cornea. The laser was focused manually to capture the corneal layers at different depths, starting from the epithelium to the maximum level with good resolution. Two examinations per eye were performed, and sequential images were documented for further analysis. HRT3 RCM uses a 670 nm laser diode and acquires an image with an area (field of view) of 400×400 µm (384 × 384 pixels), lateral optical resolution of 2 µm, and axial resolution of about 4 µm (Heidelberg Engineering, information module). After capturing each location across the corneal layers, eight distinct IVCM images were selected, representing the microstructural findings observed in the MCD patients compared to the control.

Histochemistry (HC) and immunohistochemistry (IHC) studies: Corneal buttons were processed and stained for the H&E (hematoxylin and eosin) stain and Alcian blue (AB) stain according to the published protocol [12]. Briefly, the tissue was fixed with 10% buffered formalin, phosphate-buffered saline (PBS) washed, and then gradually dehydrated with ethanol, followed by xylene-mediated clearing, and finally embedded in paraffin blocks. Using a microtome (Leica RM2255, Germany), 5 µm serial sections were made and attached to slides coated with poly-l-lysine (Polysciences, Warrington, PA). Later, the sections were dewaxed using xylene, rehydrated, and subsequently underwent haematoxylin and eosin staining and AB (pH 2.5) staining. These sections were observed using a phase contrast microscope (Nikon Eclipse Ti2, Tokyo, Japan), and an inverted phase contrast microscope (Nikon Eclipse TS100) and analyzed for GAG deposits (herein, corneal KS).

Immunostaining was performed on the deparaffinized and rehydrated sections, followed by antigen retrieval in citrate buffer (10 mM, pH 6.0) for 20 min at 95–100 °C. Later, the slides were allowed to cool down to room temperature (RT), PBS washed, and the sections were blocked with avidin-biotin (DAKO, Glostrup, Denmark) at RT. Slides were incubated overnight with mouse monoclonal 5D4 primary antibody against human KS (cat No. CAC-PRPG-BC-M01; Cosmo Bio Co. Ltd., Tokyo, Japan; 1:100 dilution) in a moist chamber at 20–25 °C. Subsequently, the slides were washed with PBS and incubated with FITC-conjugated secondary antibody (FITC-F0257-anti-mouse IgG, Sigma-Aldrich; 1:200 dilution) at 20–25 °C for 1 h, followed by a PBS wash. A Vectashield mounting medium containing propidium iodide (PI; Vector Laboratories, Burlingame, CA) was used for mounting. Immunostained sections were visualized using a confocal laser scanning microscope (Leica SP8 confocal microscope, Germany). The processed sections without primary antibodies were taken as a negative control. The expression of corneal KS was checked using three biological replicates, which showed consistent findings.

Statistical analysis: The study used ImageJ software (version 1.8.0) to quantify both epithelial and keratocyte cells. GraphPad Prism (GraphPad software version 10.1.2, La Jolla, CA) was used to perform statistical analysis and generate scatter plots for the CCT, corneal epithelial thickness, corneal epithelial cell count, and stromal keratocyte cell count of MCD patients with missense and truncating mutations compared to the control individuals. The immunohistochemistry data were analyzed using the Kruskal–Wallis test and one-way ANOVA. A p-value of <0.05 was considered statistically significant.

Quantification of keratan sulfate in serum samples: The serum KS levels were evaluated for MCD patients (n = 27) based on a competitive immunoassay using a Keratan sulfate ELISA kit (OKEH02547, Aviva Systems Biology), as per the manufacturer's protocol. Each sample was tested in duplicate. In brief, serum samples were collected using a serum separator tube and allowed to clot for 2 h at RT or overnight at 4 °C. Afterward, serum was separated by centrifugation at 503 ×g for 15 min and stored at −80 °C until further analysis. This assay consisted of a microtiter well plate precoated with anti-KS antibodies. Fifty microliters of 1X biotinylated KS were added to the wells together with the study samples or standards.

Due to the limited binding sites available on the immobilized anti-KS antibody, competition between biotinylated KS and KS present in the sample or standards was present, resulting in the washing of unbound KS. Furthermore, the addition of the tetramethylbenzidine (TMB) substrate to the Avidin-HRP conjugate during the experiment catalyzes an enzymatic reaction, producing a blue-colored product that further changes to a yellow color upon adding a stop solution (acidic nature). The density of this yellow product was measured at 450 nm (the absorbance value), which was proportional to the captured biotinylated KS amount and the inverse of the KS present in the study sample.

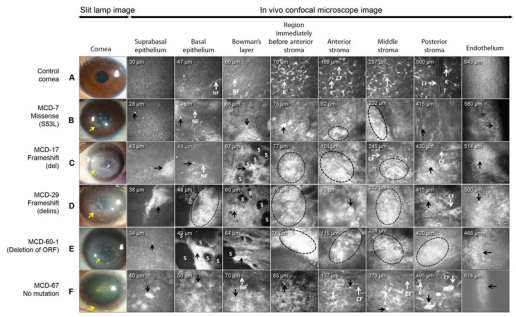

Figure 1. Slit-lamp and IVCM images of MCD patients with different CHST6 mutation types. Slit-lamp and sequential in vivo confocal images of a healthy subject (**A**-control) and selected MCD patients (**B**–**F**), representing different corneal layers. Marked corneal layers are the suprabasal epithelium, BE, Bowman's layer (BL), region immediately before anterior stroma, anterior stroma, middle stroma, posterior stroma, and endothelium. A slit-lamp and sequential IVCM analysis of the control eye showed normal cellular morphology of the different corneal layers. Suprabasal epithelium, BE of MCD patients - **B**, **C**, and **F** show scattered deposits and slightly altered nerve fibers (NF); **D** with cluster of deposits and loss of NF; and patient E (MCD patient with ORF deletion) shows clumps of deposits with scar tissue (S) and loss of NF. BL and region next to the anterior stroma of patients B and F show deposits along with loss of NF; Patients C, and D show confluent, clumps of deposits with scar tissue (S); Patient E showed clumps of highly reflective homogenous granular deposits with the rupture of basement membrane and loss of BL resulting in scar tissue. The endotheliums of Patients B and F show scattered deposits; Patients C, D, and E showed deposits along with polymegathism. Homogenous reflective material with dark striae (St)-like images was observed throughout the stroma (for patients **B**-**F**). Striae-like observations were not clearly visible due to the highly light-reflective clumps of deposits (**E**). Clinical and IVCM analysis across the corneal thickness of MCD patients 17 (**C**), 29 (**D**), and 60–1 (**E**) carrying fs deletion (del), deletion-insertion (delins), and deletion of ORF mutations, respectively, revealed severe scars in the BL and anterior stroma due to highly light-reflective clumps of deposits presenting severe corneal morphological alterations.

CHST6 mutational screening and in silico analysis: A polymerase chain reaction was performed for the amplification of exon 3 of the CHST6 gene, followed by bidirectional Sanger sequencing (ABI 3130 genetic analyzer, Applied Biosystems, Foster City, CA), as per previously published methods and conditions [3]. Sequencing results were analyzed using Chromas Lite (2.1) software and compared with the CHST6 reference sequence using the Basic Local Alignment Search Tool (BLAST).

Sorting intolerant from tolerant (SIFT), polymorphism phenotyping (PolyPhen), and mutation taster were used to predict the pathogenicity of an identified novel mutation. The evolutionary conservation of the novel mutation was analyzed using the ClustalW multiple sequence alignment tool. Furthermore, the prediction of the secondary structure of the CHST6 protein was performed using the Self-Optimized Prediction Method with Alignment (SOPMA) tool. It provides information on the alpha helix, beta sheet, extended strand, Pi helix, coil, etc.

RESULTS

A collective investigation into the clinical and genetic attributes of individuals diagnosed with MCD revealed a diffuse stromal haze characterized by the accumulation of irregular gray-white deposits featuring indistinct edges. Moreover, the intervening stroma exhibited an unclear appearance (Figure 1 and Appendix 1). Furthermore, this study identified 18 distinct pathogenic mutations in the CHST6 gene associated with MCD disease phenotypes.

This current study focused on 68 Indian patients presenting with MCD phenotypes. Among them, there were 34 males and 34 females, with the mean age of disease presentation recorded as 35.3 ± 11.3 years. Pedigree analysis showed that 50% (n = 34) of the study patients were born to consanguineous parents, while 45.5% (n = 31) displayed a family history. Furthermore, genetic analysis uncovered various mutations in the CHST6 gene. Specifically, 51.5% (n = 35) of the patients harbored 11 distinct homozygous missense mutations, including p.R50C, p.S53L, p.R93H, p.R127C, p.L129V**,** p.S131P, p.R202H, p.R205Q, p.R205W, p.D221, and p.E274Q; 16.2% (n = 11) showed homozygous deletion mutation (p.F60LfsX10, p.V66VfsX3, p.F67SfsX3, and p.Q182RfsX199); 5.9% (n = 4) had heterozygous deletion (p.Q182RfsX199, and p.V66VfsX3); 1.5% (n = 1) carried a heterozygous missense mutation (p.R50C); 1.5% (n = 1) displayed a nonsense mutation (p.S81X); 4.4% (n = 3) found with replacement and deletion mutation (p.N194_R196delinsRC) and 7.4% (n = 5) exhibited deletions of the open reading frame (ORF; Table 1).

Table 1. *CHST6* mutations identified in the MCD families.

Mutation type	Mutation details	No. of families	No. of patients
Missense	c.148C>T (p.R50C)	4	4
	c.158C>T (p.S53L)	15	18
	c.278G>A (p.R93H)	6	7
	c.379C>T (p.R127C)	2	2
	c.385C>G (p.L129V)	1	2
	c.391C>T (p.S131P)	1	1
	c.290 G>A (p.R202H)	1	1
	c.614G>A (p.R205Q)	3	3
	c.613C>T (p.R205W)	1	1
	c.843C>G (p.D221E)	1	1
	c.820G >C (p.E274Q)	1	1
Nonsense	c.242C>A (p.S81X)	1	1
	c.180delC (p.F60LfsX10)	2	2
Frameshift (del)	c.198delC (p.V66VfsX3)	1	1
	c.199T>A (p.F67SfsX3)	1	1
	c.545delA (p.Q182RfsX199)	11	12
Frameshift (delins)	c.581_586delACCTACinsGGTN (p.194_R196delinsRC)	3	4
	Deletion of ORF	5	10

Sixty-eight families consisting of 68 probands and available family members were genetically screened. Eight families did not harbor *CHST6* gene mutations. Mutation p.L129V marked in bold represents a novel mutation identified in the present study. *CHST6*- carbohydrate sulfotransferase gene; MCD- Macular corneal dystrophy; del-deletions; delins- deletion-insertion; ORF- Open reading frame. Additional details of the identified mutations in the study participants are given in the Appendix 1.

The pathogenicity of a mutation was determined using Insilico tools, including SIFT, Polyphen2, and Mutation Taster, according to the ACMG guidelines of the American College of Medical Genetics and Genomics (ACMG). Notably, eight patients did not harbor any mutations in the CHST6 gene. The complete details of the mutations identified in the patients and their family members are given in Appendix 2. Also, variations within the amino acid R-group are delineated as follows: acidic to acidic (n = 1); basic to basic (n = 7); acidic to polar (n = 1); basic to polar (n = 9); polar to basic (n = 3); polar to nonpolar (n = 16); basic to nonpolar (n = 1); nonpolar to nonpolar (n = 1); frameshift mutation (n = 15); deletion ORF (n = 5); and nonsense mutation (n = 1). Interestingly, this study identified a novel homozygous missense mutation (p.L129V) in the CHST6 gene. Subsequently, multiple sequence analysis of the novel variant showed an impact on the highly conserved amino acid residue leucine (L) at position 129 (Appendix 3). The SOPMA analysis of the novel mutant demonstrated a significant alteration in its secondary protein structure compared to the control. Specifically, there was an increase in alpha helix, a reduction in extended strand, a rise in beta-turn, and a decrease in random coil formation (Appendix 3).

Furthermore, this study also conducted IVCM, histochemistry, immunohistochemistry, and ELISA analyses on 25 MCD patients and two family members (comprising 14 males and 13 females, with a mean age of 40.1 years ± 12.8). Ten age-matched healthy individuals were included as controls for comparison.

Corneal architecture analysis by in vivo confocal microscopy: The MCD patients carrying missense mutations (Patients 7, 14, 30, 35, 36, 40, 48, and 52) exhibited microstructural changes across various corneal layers, as delineated in Appendix 4. Specifically, the findings for Patient 7 with the S53L mutation and the control cornea from healthy subjects are depicted in Figure 1. IVCM analysis of MCD patients with missense mutations showed consistent structural changes, including highly reflective scattered deposits with defined borders in the basal epithelium (BE). Also, the reduced density of long nerve fibers (NF) and the presence of abnormal short nerve fibers were observed, along with

the highly reflective clumps of deposits in the BE and BL (Figure 1). Bright, light-reflective diffuse deposits, along with striae (St), were seen in the superficial, anterior, middle, and posterior stroma (S). Furthermore, uneven scattered deposits were observed in the corneal endothelium (EN).

The IVCM of patients harboring a deletion mutation (Appendix 4, Patient IDs 11, 17, 25, 41, 61, 64, 65, and 66) showed highly reflective clumps of depositions in the suprabasal epithelium, BL, along with abnormal, short NF without branching (Patient 17, Figure 1). The BL was not clear due to scar tissue (S). A cluster of highly reflective, bright, diffuse deposits was seen throughout the stroma, along with dark striae (St), a lesser number of keratocytes (K), and abnormal collagen lamellae. Uneven, light-reflective scattered deposits were observed in the endothelium, leading to polymegathism.

Assessments of corneal structural changes for the patients carrying the delins mutation (Patient IDs 24 and 29) through IVCM are given in Appendix 4. IVCM images for Patient 29 are shown in Figure 1, where bright, highly light-reflective homogenous granular deposits were seen in the suprabasal, BE, and BL, along with a complete loss of NF in the BE and BL. A light-reflective cluster of deposits was noted in the stroma. The presence of striae was observed, although they were not clearly visible in these patients due to highly reflective deposits. Moreover, BL was not clear, with scar tissue (S) extending from the basal membrane to the underlying stroma. Furthermore, abnormal structures of collagen lamellae were also seen, along with the loss of keratocyte cells. Polymegathism was observed in the endothelium along with scattered deposits.

MCD patients detected with the ORF deletion mutation (Patient IDs 49–1, 49–2, 60–1, 60–2, and 68; Appendix 4) had progressive bilateral visual loss (only hand movement), and IVCM scanning revealed the same aforementioned changes (i.e., presence of a scar, endothelial polymegathism, etc.) as observed in MCD Patient 29 with the delins mutation. Also, a large light-reflected cluster of deposits with irregular edges was seen immediately after the BL and before the anterior stroma (Patient 60–1, Figure 1).

Patients who were negative for the CHST6 mutation (Patient IDs 5, 56, 63, and 67) presented with the MCD phenotype (Figure 1) and had difficulty visioning (Appendix 2 and Appendix 4). IVCM analysis of Patient 67 showed a fine, light-reflective cluster of abnormal deposits in the suprabasal epithelium, with clear, bright borders, distinct nuclei, and dark cytoplasm (Figure 1). A wing-like flattened deposit was seen in the BE and BL, with abnormal and short NF. Furthermore, highly light-reflective diffuse deposits were observed throughout the anterior, middle, and posterior stroma with the loss of keratocytes. A faint deposit was also seen in the corneal endothelium.

Histochemistry and immunohistochemistry analysis: Histological corneal sections stained with AB from MCD patients identified with missense mutations revealed blue-stained GAG deposits in the epithelium, stromal keratocytes, and stromal lamellae (Figure 2). These deposits were found in the endothelial cells lining Descemet's membrane. Additionally, some abnormal keratocytes were observed in the anterior stroma compared to the sections observed in the control group. AB-stained corneal sections for the patients with del mutations showed BL destruction due to abnormal superficial deposits, along with abnormal keratocytes in the middle and posterior stroma. Furthermore, patients harboring CHST6 delins and ORF deletion mutations typically manifested severe morphological changes in the cornea, including thin, irregular, and attenuated epithelium, along with focal breaks and destruction of BL. In comparison to the control group, these patients also exhibited a 2- to 3-fold decrease in stromal thickness and disorganization of the collagen lamellae. Additionally, there were diffuse, subepithelial, and stromal interlamellar irregular GAG deposits along with abnormal keratocytes. Although Descemet's membrane remained intact, it was considerably thickened. The corneal endothelial cells were either absent or markedly reduced and were highly abnormal.

The immunostaining of corneal sections from the patients with distinct missense mutations showed an absence of KS expression (negative immunoreactivity to anti-KS 5D4 MoAb) throughout the entire cornea, including the stroma, stromal lamellae, keratocytes, Descemet's membrane, and endothelium (Figure 2). Consequently, this phenotype was categorized as immunophenotype I (Appendix 4). Furthermore, patients with this immunophenotype exhibited a reduced mean central corneal thickness (344 µm) compared to the controls (480 µm). The patients with frameshift deletions, delins mutations, and deletions of the ORF exhibited severe corneal morphological alterations, with mean CCT thicknesses of 301 µm, 194 µm, and 243 µm, respectively. Subsequently, this phenotype was classified under immunophenotype IA due to faint KS expression perceived only in the stromal keratocytes, while the other corneal layers showed no KS expression (no immunoreactivity).

BL destruction was observed in the central cornea, whereas the peripheral cornea was normal (Figure 2). Altogether, the patients with truncation mutations (frameshift del, delins, deletion of ORF) showed significantly reduced CCT (p-value < 0.001) as compared to the controls (Figure 3). Patients lacking CHST6 mutations were categorized

under immunophenotype II, as they were observed with slightly reduced KS expression across the stroma, Descemet's membrane, and endothelium. These patients also displayed a reduced mean CCT of 336 µm.

This study also quantified the corneal epithelial cell count and epithelial thickness to understand the structural arrangements of the cornea in MCD patients. Notably, a significant decrease (p-value < 0.001) in both epithelial

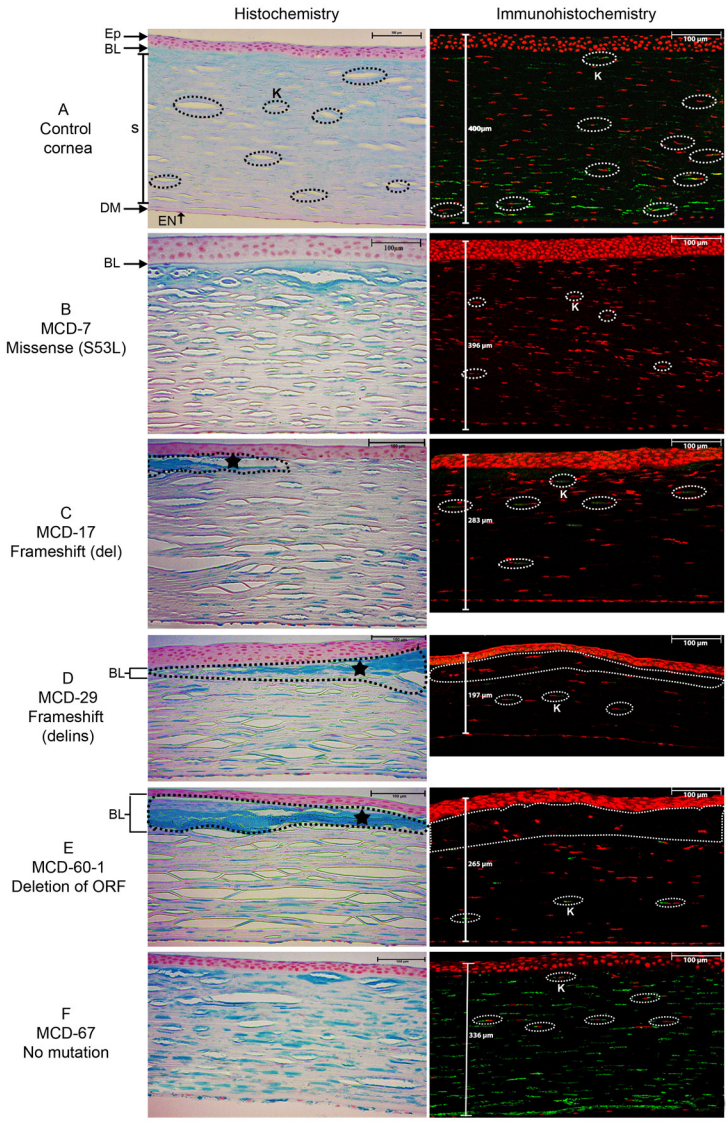

Figure 2. Representative images of corneal sections for histochemistry (HC-AB staining) and immunohistochemistry (IHC-5D4 MoAb immunoreactivity) analysis of normal (control) and MCD patients with different mutation types. Images on the left side represent AB-stained corneal sections, and the right side represents immunostained sections. **A**: The corneal layers marked in the control (cadaver) show normal morphology. **B**–**F** represent images of unrelated MCD patients (Patients 7, 17, 29, 60–1, and 67) harboring different CHST6 mutations. Major changes were observed for the patients harboring deletion (del), deletion-insertion (delins), and deletion of ORF mutations with severe morphological alterations in the BL and anterior stroma due to abnormal, amorphous, finely granulated GAG deposits (*) with altered collagen lamellae and altered keratocyte (K) cell shape. IHC also showed the presence of KS only in the stroma, with a smaller number of stromal keratocytes. **F** represents the images for the MCD patient with no coding region CHST6 mutation, showing a normal corneal morphology like the control (**A**). In the IHC images, red represents PI staining, and green indicates FITC-labeled anti-KS antibodies. Ep, epithelium; BL, Bowman's layer; BM, basement membrane; S, stroma; DM, Descemet's membrane; EN, endothelium; K, keratocytes.

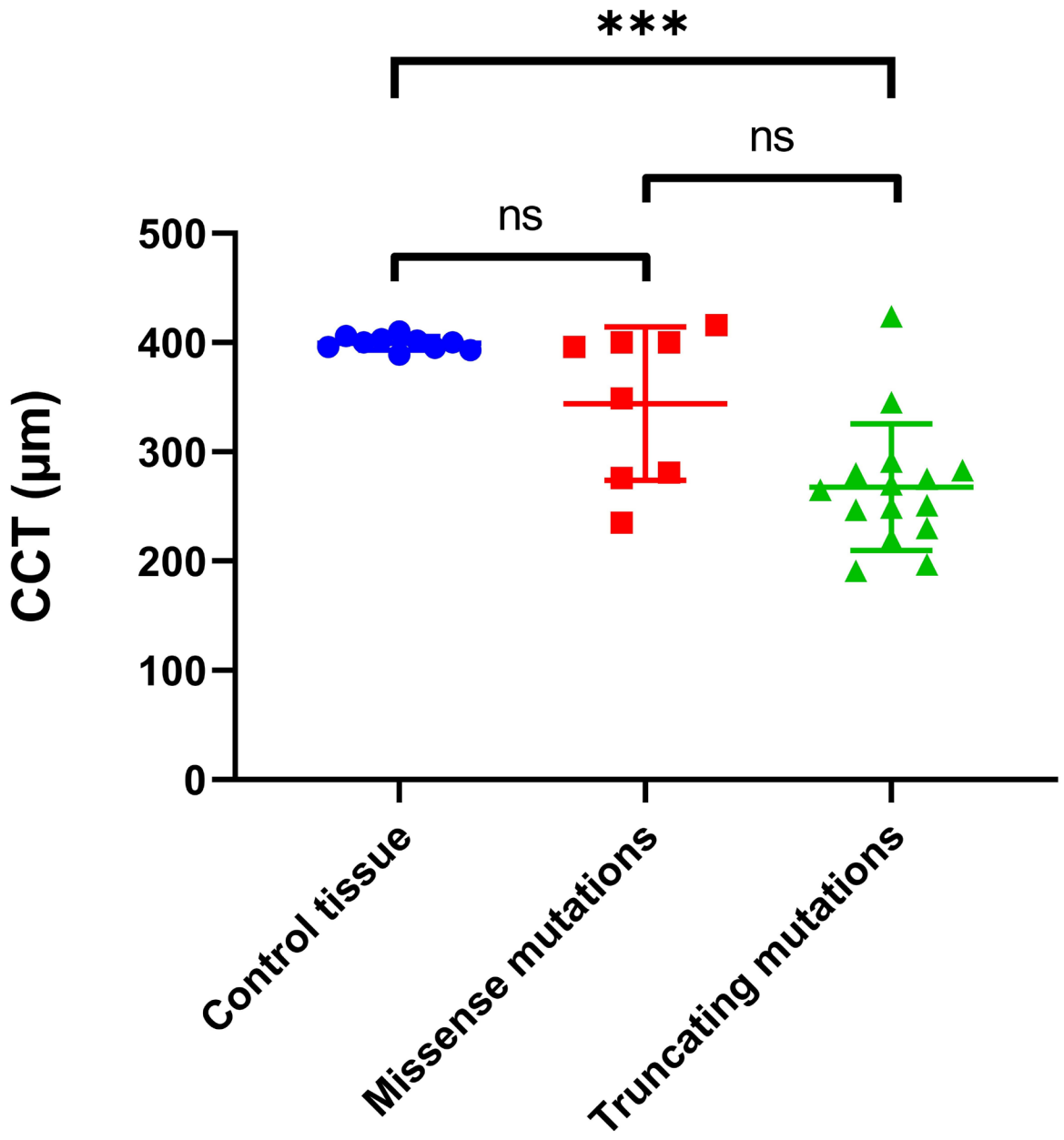

Figure 3. Comparison of the central corneal thickness of MCD patients and the control group. Scatter plots show significantly reduced central corneal thickness in patients with truncation mutations compared to the control group. Quantitative analysis among the groups was performed using a one-way ANOVA. A p-value of less than 0.001 (***) was considered statistically significant (ns, not significant).

thickness (Figure 4A) and epithelial cell count (Figure 4B) was revealed in the patients with truncation mutations compared to controls. Also, there was significance (p-value < 0.05) seen between the missense and truncation groups for epithelial cell count and epithelial thickness. However, the study did not observe significant differences between the missense and control groups.

Further, the quantitative analysis also displayed a significant reduction (p-value < 0.001) in stromal keratocyte cell count among the patients with truncation mutations compared to the controls, as depicted in Figure 5. There was

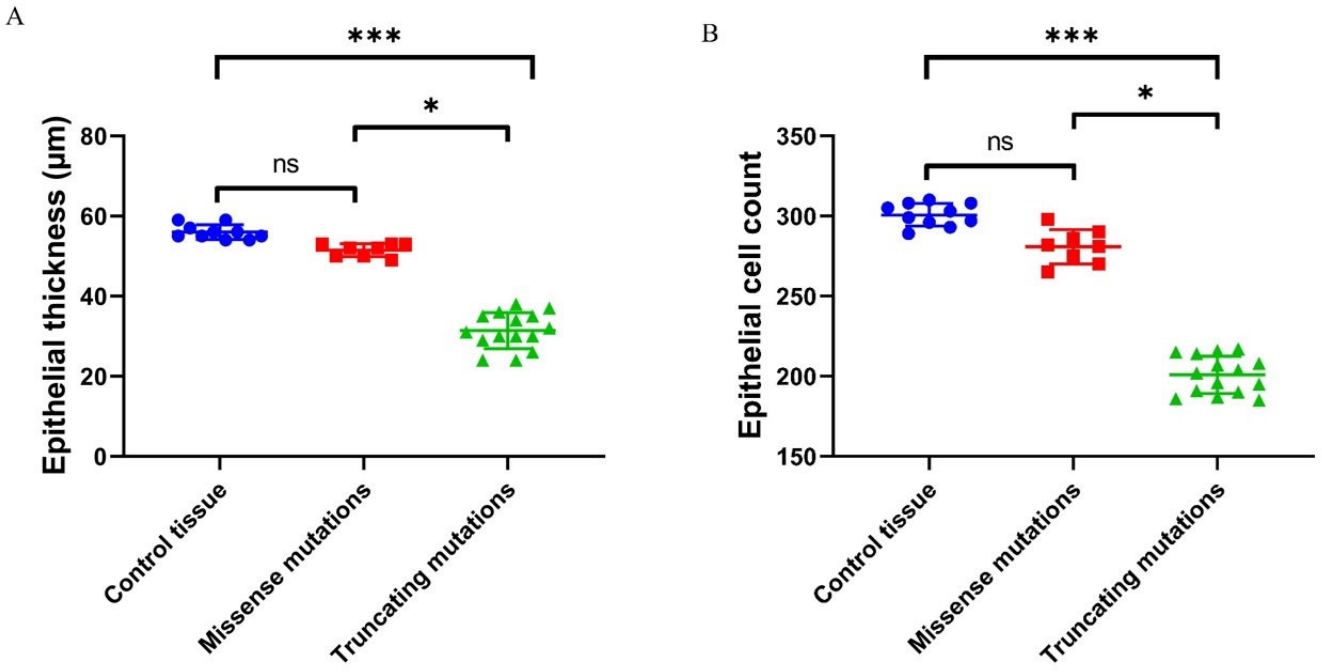

Figure 4. Comparison of corneal epithelial thickness and corneal epithelial cell count among MCD patients and the control group. **A**: Scatter plot shows a significantly reduced corneal epithelial thickness observed in the patients with truncation mutations compared to the control group. **B**: A significantly reduced count of corneal epithelial cells was observed in the patients with truncation mutations compared to the control group. Quantification among the groups was performed using a one-way ANOVA. A p-value of less than 0.001 (***) and a p-value of less than 0.05 (*) were considered statistically significant. (ns-not significant).

significance (p-value < 0.05) seen between the missense and truncation groups for stromal keratocyte cell count. However, the study did not observe significant differences between the missense and control groups.

Serum keratan sulfate level analysis: An ELISA was performed to ascertain the serum keratan sulfate (KS) level in individuals with distinct MCD immunophenotypes (n = 27; Appendix 4). The average serum KS levels were 350±40 ng/ml for the control group. Among MCD patients, those classified under immunophenotype I (n = 8) exhibited mean serum KS levels of 1.37 ± 0.38 ng/ml, while patients categorized as immunophenotype IA (n = 15) showed mean KS levels of 5.43 ± 1.95 ng/ml. The patients with immunophenotype II MCD (n = 4) had mean serum KS levels of 115.5 ± 11.73 ng/ml. Our findings suggest that individuals classified under immunophenotypes I and IA showed significantly lower serum KS levels compared to those in Type II and the control group.

DISCUSSION

MCD is a disease of KS metabolism, where KS is a major corneal glycosaminoglycan (GAG) involved in the organization of collagen fibrils [13]. An ordered lattice structure of regular interspaced, tightly packed collagen fibrils in the corneal stroma is the cardinal requirement for optical clarity and, hence, transparency. The importance of KS sulfation, mediated by corneal sulfotransferases, is crucial for bridge formation. Abnormally sulfated or unsulfated KS between collagen fibrils fails to form bridges, resulting in a disturbed lattice arrangement and reduced interfibrillar spacing, thus reducing corneal thickness in MCD corneas compared to normal corneas [14]. Genetic mutations in the CHST6 gene result in fluctuations in KS sulfation activity across the cornea and other tissue types [12].

CHST6 has two highly conserved sites for the 3′-phosphoadenosine 5′-phosphosulphate (PAPS) binding. One is the 5-phosphosulfate binding site (5-PSB) and another is the RX7S 3-phosphate binding site (3-PB) in the C terminus for the catalytic activity of the corneal glucosamine N-acetyl-6-sulfotransferase (C-GlcNAc6ST). These sites play a crucial role in determining carbohydrate specificity and sulfation, orchestrating the precise transfer of sulfate to position 6-O of the N-acetylglucosamine moiety within the keratan structure of corneal tissue [5,13]. Moreover, it has been shown that corneal N-acetyl glucosamine 6-sulfotransferase catalyzes

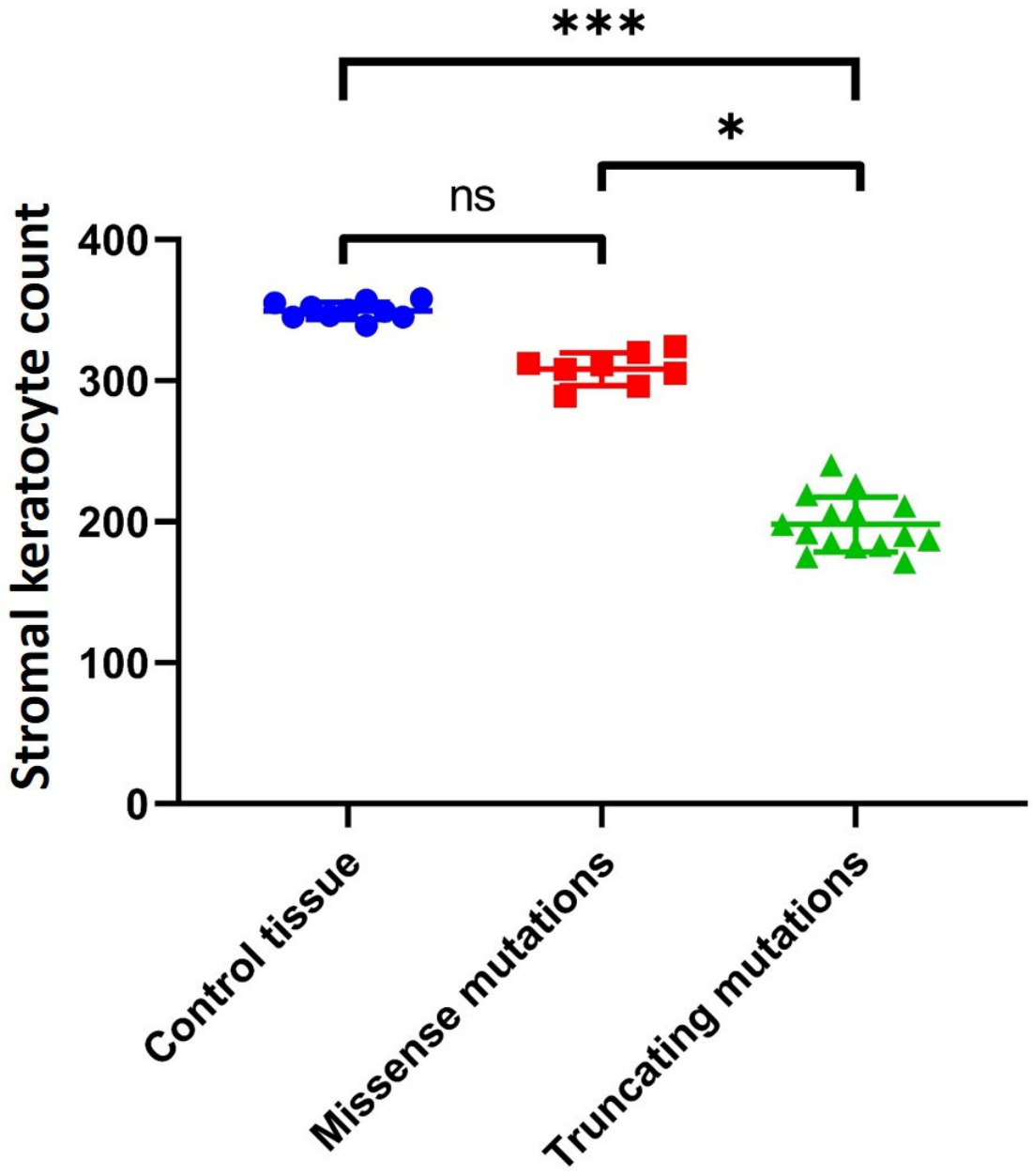

Figure 5. Comparison of stromal keratocyte cell counts among MCD patients and the control group**.** The scatter plot shows a significantly reduced count of corneal stromal cells in the patients with truncation mutations compared to the control group. Quantification among the groups was performed using a one-way ANOVA. A p-value of less than 0.001 (***) and a p-value of less than 0.05 (*) were considered statistically significant. (ns-not significant).

the 6-O-sulfation of endothelial mucin efficiently, the activity known for intestinal N-acetyl glucosamine sulfotransferase [15]. Hence, biochemical assessments of CHST6 enzymatic activity in patients with various CHST6 mutations and immunophenotypes will offer further insights into the observed changes in corneal sections.

This study aimed to provide comprehensive insight into the CHST6 mutational spectrum and corneal cellular structure using IVCM, histochemistry, immunohistochemistry

analysis, and serum KS levels in MCD patients to gain a deeper understanding of the pathogenesis among individuals of Indian origin. In the present study, 50% of the MCD patients were born to consanguineous parents. Earlier reports indicate that the frequent practice of consanguineous and endogamous marriages within communities in India is often linked to the occurrence of the MCD phenotype [16]. The mean age of the patients included in this study was approximately 35.3 ± 11.3 years, which aligns with findings from previous studies on MCD [8]. In total, the current study identified 17 distinct mutations and one novel missense variant in the CHST6 gene. All of these identified mutations in the CHST6 gene, including missense, frameshift, nonsense, delins, and deletions of ORF, are considered pathogenic. Prior studies have indicated that individuals harboring these mutations are predisposed to distinct MCD phenotypes [13,14]. Interestingly, the present study also identified a novel homozygous missense mutation (p.L129V) in the CHST6 gene, displaying the MCD phenotype, yet its functional significance in MCD pathogenesis remains unclear. Further functional studies are needed to observe the effects of novel variants on MCD pathogenesis.

Notably, eight patients displayed the clinical phenotype of MCD despite the absence of any mutations in the CHST6 gene. Of these eight patients, segregation analysis was done for the two MCD patients (MCD-56–1 and MCD-63–1) with available family members. Both MCD patients had a positive family history and consanguinity. Also, we did not observe the segregation of the CHST6 marker in the family members (Appendix 2). This underscores the significance of next-generation sequencing in investigating the additional genetic factors associated with MCD. It is conceivable that these patients may carry hypomorphic variants or deep intronic variants in the CHST6 gene, contributing to the manifestation of the disease phenotype. Studies have shown that MCD patients without CHST6 mutations exhibit genomic changes in transcription factor binding sites or other cis-regulatory elements, including enhancers and repressors, affecting keratan sulfation [2,3,17].

The importance of corneal IVCM assessments has been understood in earlier studies. For instance, Kobayashi et al. performed IVCM on 2 MCD patients (with A217T mutation), which showed hyper-reflective deposits without distinct borders in the epithelial layer and positive AB staining corresponding to mucopolysaccharide presence [18]. The light-reflected deposits in the BE were also observed in the present study, along with the endothelial scattered deposits and polymegathism in the patients harboring CHST6 truncation mutations.

A study by Muller et al. showed that, in general, nerve plexus/fibers were more frequently visible in the central cornea than in the peripheral region [19]. In the current study, abnormal, very short, or complete loss of NF in the BE and BL was observed in the patients carrying the truncation mutation, while a reduced density of long NF and abnormal short NF was present in the patients with missense mutations. This further suggests a more affected central cornea than the peripheral region, thus observing central corneal thinning in these patients. Moreover, the study also observed significantly reduced CCT in patients with truncation mutations (frameshift del, delins, deletion of ORF) compared to the controls. Also, BL and the surrounding tissues are not clearly visible due to highly reflective clumps of granular deposits together with noticeable scar tissue in patients with truncation mutations.

Bright oval or bean-shaped quiescent keratocyte nuclei are generally observed in the stroma of the cadaver cornea [20–23]. However, during wound healing, activated keratocytes have been observed to have a large, highly reflective appearance [24–27]. Similar features were noted in our study of patients who were suspected to have CHST6 truncation mutations, suggesting that more wound healing might have occurred in these patients. The presence of deposits seen in MCD patients results in the irregular arrangement of collagen fibers, which were observed to have dark striae-like appearances throughout the stroma. This striae-like feature of collagen fibers, together with a reduction in interfibrillar spaces, is possibly responsible for the reduced corneal thickness observed in our study patients, especially in patients with truncation mutations. A study by Niel et al. suggested that CHST6 frameshift mutations may lead to severe MCD phenotypes with much deeper deposits [1].

An analysis of corneal morphology by AB staining and an immunohistochemical investigation of the KS immunoreactivity in the corneal sections revealed thin epithelium and thick BL with focal rupture or destruction, along with abnormal keratocytes, in the patients with truncation mutations. Furthermore, alterations, including severe scars in the BL and anterior stroma, were observed using IVCM analysis. Moreover, a quantitative analysis of the epithelial thickness, epithelial cell counts, and stromal keratocyte counts in patients harboring truncation mutations showed a significant decrease compared to the controls. Depletion of BL and normal morphology of keratocytes were observed in patients with missense mutations. Earlier studies suggested BL with some discontinuities together with clusters of abnormal, anomalous granular material, which could correspond to the

irregular hyper-reflective areas observed on IVCM analysis [28–32].

Sultana et al. reported that MCD Type I was the predominant immunophenotype in Indian patients [12]. However, their study revealed no correlation between immunophenotypes and specific CHST6 mutations. In current study, a greater number of patients were observed under MCD immunophenotype IA (55.6%) who harbored either truncation mutations with noticeable severe corneal structural changes. Patients with immunophenotype I (29.6%) harbored missense mutations, and four patients (14.8%) who did not carry CHST6 coding region mutations had KS expression patterns consistent with immunophenotype II. This current study on Indian MCD subjects showed a predominance of immunophenotype IA, followed by immunophenotypes I and II.

Earlier studies on a few patients looked for KS in serum or corneal sections, CHST6 gene screening, and corneal structural changes, yet not altogether [32–34]. For instance, Nowinska et al. used confocal microscopy to study 24 Polish MCD patients for their corneal morphological organization and their study used 10 corneal buttons for histological and CHST6 mutational analyses [35]. The study identified different missense mutations alone, revealing genetic mutation heterogeneity; however, no phenotype heterogeneity was observed. Additionally, their study did not investigate AgKS expression in corneal sections or serum KS levels.

This present study collectively provides valuable insight into the potential repercussions of CHST6 mutations associated with MCD on the corneal microstructure. Additionally, quantitative measurements showed significant changes in the corneal epithelium thickness, epithelial cell count, and keratocyte count in patients with truncations. However, further studies involving a larger sample size are warranted to substantiate these findings.

Conclusion: This is the first study in India that represents a comprehensive investigation of MCD patients. It unveiled a distinctive correlation between truncation mutations and pronounced changes in the corneal microstructure. Furthermore, this study uncovered a novel missense mutation, thus expanding the CHST6 mutational landscape of MCD. Our findings also highlight the predominance of immunophenotype IA among Indian MCD patients. Moreover, this study underscores the importance of screening CHST6 mutations for precise molecular diagnosis and of providing valuable counseling for families affected by MCD.

APPENDIX 1. SUPPLEMENTARY FIGURE 2.

To access the data, click or select the words "Appendix 1." Slit lamp images of patients harboring different *CHST6* mutations. Slit lamp photograph of all MCD patients showing irregular hazy, gray-white opacities (yellow arrows). On the top of the image (white numbers) first number represents MCD patient ID followed by age and sex. A- Different missense mutations, B- Different deletion mutation, C- Deletion insertion mutation, D- ORF deletion mutation, E- Negative mutation.

APPENDIX 2. SUPPLEMENTARY TABLE 1.

To access the data, click or select the words "Appendix 2." Details of the *CHST6* mutations identified among 68 MCD patients and their family members.

APPENDIX 3. SUPPLEMENTARY FIGURE 1.

To access the data, click or select the words "Appendix 3." Family Pedigree, sequencing chromatograms, SOPMA and Multiple Sequence Alignment (MSA) results for the novel mutation c.385C>G, p.L129V identified in MCD family 55. (A) Pedigree showing the male patient (filled black square with arrow, IV:1- proband), affected sibling (filled black square, IV:2) and parents (father-III:3; mother- III:4). Squares represent men and circles for women. Double line in the pedigree show consanguineous marriage and red star marks represents the subjects underwent *CHST6* mutation screening. (B) Representative chromatograms for the normal control (wild-type genotype), MCD patient (IV:1) and his sibling (IV:2) harbor homozygous mutation c.385C>G (p.L129V) in *CHST6* gene, while parents (III:3, III:4) carried mutation in heterozygous condition. (C) Secondary structure prediction by SOPMA (Self-Optimized Prediction Method with Alignment) tool. SOPMA predicted that the mutated protein (p.L129V) had altered secondary protein structure (i.e., increased alpha helix, decreased extended strand, increased beta turn, decreased random coil) when compared to the control, suggesting the formation of unstable protein. (D) Evolutionary conservation for the mutation p.L129V was assessed using ClustalW (1.2.2) MSA tool which showed the highly conserved nature of the leucine (L) amino acid residue at position 129 (marked in red box).

APPENDIX 4. SUPPLEMENTARY TABLE 2.

To access the data, click or select the words "Appendix 4." Histochemistry, immunohistochemistry, IVCM, and immunophenotype findings of individuals harboring varied *CHST6* mutations.

ACKNOWLEDGMENTS

The authors are grateful to the study subjects for their participation in this study. We thank clinicians who were involved in patient screening and laboratory assistants who helped for sample collection. We thank statisticians, and bioinformaticians who helped with data analysis. FUNDING: This work was supported by the Department of Science and Technology-INSPIRE fellowship 2015 Grant No. IF150303, New Delhi, India, and a research grant (MUTT study 1) from Aravind Eye Care System, Madurai, Tamil Nadu, India. DECLARATION OF INTERESTS: The authors report no conflicts of interest.

REFERENCES

1. Niel F, Ellies P, Dighiero P, Soria J, Sabbagh C, San C, Renard G, Delpech M, Valleix S. Truncating mutations in the carbohydrate sulfotransferase 6 gene (CHST6) result in macular corneal dystrophy. Invest Ophthalmol Vis Sci 2003; 44:2949-53. [PMID: 12824236].
2. Warren JF, Aldave AJ, Srinivasan M, Thonar EJ, Kumar AB, Cevallos V, Whitcher JP, Margolis TP. Novel mutations in the CHST6 gene associated with macular corneal dystrophy in southern India. Arch Ophthalmol 2003; 121:1608-12. [PMID: 14609920].
3. Murugan D, Prajna NV, Devi L, Sundaresan P. Genetic Analysis of CHST6 Gene in Indian Families with Macular Corneal Dystrophy. Int J Gen Sci.2017: 4:1–10. Surv Ophthalmol 2018; 63:609-17. .
4. Aggarwal S, Peck T, Golen J, Karcioglu ZA. Macular corneal dystrophy: A review. Surv Ophthalmol 2018; 63:609-17. [PMID: 29604391].
5. Wang L, Tang X, Lv X, Sun E, Wu D, Wang C, Liu P. *CHST6* mutation screening and endoplasmatic reticulum stress in macular corneal dystrophy. Oncotarget 2017; 8:96301-12. doi:10.18632/oncotarget.22028[PMID: 29221207].
6. Klintworth GK, Jester JV. Genetic basis of corneal diseases and the role of keratocytes in corneal transparency–a review. Clin Exp Ophthalmol 2010; 38:23-33. .
7. Kaarniranta K, Szalai E, Smedowski A, Hegyi Z, Kivinen N, Viiri J, Wowra B, Dobrowolski D, Módis L Jr, Berta A, Wylegala E, Felszeghy S. A novel proteotoxic stress associated mechanism for macular corneal dystrophy. Histol Histopathol 2015; 30:921-30. [PMID: 25597745].
8. Sultana A, Sridhar MS, Jagannathan A, Balasubramanian D, Kannabiran C, Klintworth GK. Novel mutations of the carbohydrate sulfotransferase-6 (CHST6) gene causing macular corneal dystrophy in India. Mol Vis 2003; 9:730-4. [PMID: 14735064].
9. Klintworth GK, Oshima E, al-Rajhi A, al-Saif A, Thonar EJ, Karcioglu ZA. Macular corneal dystrophy in Saudi Arabia: a study of 56 cases and recognition of a new immunophenotype. Am J Ophthalmol 1997; 124:9-18. [PMID: 9222226].
10. Alhatem A, Cavalcanti B, Hamrah P. In vivo confocal microscopy in dry eye disease and related conditions. Semin Ophthalmol 2012; 27:138-48. [PMID: 23163268].
11. Miller SA, Dykes DD, Polesky HF. A simple salting out procedure for extracting DNA from human nucleated cells. Nucleic Acids Res 1988; 16:1215-[PMID: 3344216].
12. Sultana A, Klintworth GK, Thonar EJ, Vemuganti GK, Kannabiran C. Immunophenotypes of macular corneal dystrophy in India and correlation with mutations in CHST6. Mol Vis 2009; 15:319-25. [PMID: 19204788].
13. Huang Y, Yuan L, Cao Y, Tang R, Xu H, Tang Z, Deng H. Novel compound heterozygous mutations in the *CHST6* gene cause macular corneal dystrophy in a Han Chinese family. Ann Transl Med 2021; 9:622- doi:10.21037/atm-20-7178[PMID: 33987320].
14. Zhang J, Wu D, Li Y, Fan Y, Dai Y, Xu J. A comprehensive evaluation of 181 reported *CHST6* variants in patients with macular corneal dystrophy. Aging (Albany NY) 2019; 11:1019-29. [PMID: 30716718].
15. Bartes A, Bhakta S, Hemmerich S. Sulfation of endothelial mucin by corneal keratan N-acetylglucosamine 6-O-sulfotransferase (GST-4β). Biochem Biophys Res Commun 2001; 282:928-33. [PMID: 11352640].
16. Sultana A, Sridhar MS, Klintworth GK, Balasubramanian D, Kannabiran C. Allelic heterogeneity of the carbohydrate sulfotransferase-6 gene in patients with macular corneal dystrophy. Clin Genet 2005; 68:454-60. [PMID: 16207214].
17. Klintworth GK, Smith CF, Bowling BL. CHST6 mutations in North American subjects with macular corneal dystrophy: a comprehensive molecular genetic review. Mol Vis 2006; 12:159-76. [PMID: 16568029].
18. Kobayashi A, Fujiki K, Fujimaki T, Murakami A, Sugiyama K. In vivo laser confocal microscopic findings of corneal stromal dystrophies. Arch Ophthalmol 2007; 125:1168-73. [PMID: 17846354].
19. Müller LJ, Vrensen GF, Pels L, Cardozo BN, Willekens B. Architecture of human corneal nerves. Invest Ophthalmol Vis Sci 1997; 38:985-94. [PMID: 9112994].
20. Müller LJ, Pels L, Vrensen GF. Novel aspects of the ultrastructural organization of human corneal keratocytes. Invest Ophthalmol Vis Sci 1995; 36:2557-67. [PMID: 7499078].
21. Mustonen RK, McDonald MB, Srivannaboon S, Tan AL, Doubrava MW, Kim CK. Normal human corneal cell populations evaluated by in vivo scanning slit confocal microscopy. Cornea 1998; 17:485-92. [PMID: 9756442].
22. Erie JC, Patel SV, McLaren JW, Maguire LJ, Ramirez M, Bourne WM. Keratocyte density in vivo after photorefractive keratectomy in humans. Trans Am Ophthalmol Soc 1999; 97:221-36. , discussion 236–40.. [PMID: 10703126].
23. Patel S, McLaren J, Hodge D, Bourne W. Normal human keratocyte density and corneal thickness measurement by using confocal microscopy in vivo. Invest Ophthalmol Vis Sci 2001; 42:333-9. [PMID: 11157863].

24. Corbett MC, Prydal JI, Verma S, Oliver KM, Pande M, Marshall J. An in vivo investigation of the structures responsible for corneal haze after photorefractive keratectomy and their effect on visual function. Ophthalmology 1996; 103:1366-80. [PMID: 8841294].

25. Møller-Pedersen T, Cavanagh HD, Petroll WM, Jester JV. Corneal haze development after PRK is regulated by volume of stromal tissue removal. Cornea 1998; 17:627-39. [PMID: 9820944].

26. Bourne WM. Cellular changes in transplanted human corneas. Cornea 2001; 20:560-9. [PMID: 11473153].

27. Mitooka K, Ramirez M, Maguire LJ, Erie JC, Patel SV, McLaren JW, Hodge DO, Bourne WM. Keratocyte density of central human cornea after laser in situ keratomileusis. Am J Ophthalmol 2002; 133:307-14. doi:10.1016/s0002-9394(01)01421-0[PMID: 11860965].

28. Snip RC, Kenyon KR, Green WR. Macular corneal dystrophy: ultrastructural pathology of corneal endothelium and Descemet's membrane. Invest Ophthalmol 1973; 12:88-97. [PMID: 4265065].

29. Santo RM, Yamaguchi T, Kanai A, Okisaka S, Nakajima A. Clinical and histopathologic features of corneal dystrophies in Japan. Ophthalmology 1995; 102:557-67. [PMID: 7724173].

30. Jonasson F, Oshima E, Thonar EJ, Smith CF, Johannsson JH, Klintworth GK. Macular corneal dystrophy in Iceland. A clinical, genealogic, and immunohistochemical study of 28 patients. Ophthalmology 1996; 103:1111-7. [PMID: 8684802].

31. Kobayashi A, Yokogawa H, Sugiyama K. In vivo laser confocal microscopy of Bowman's layer of the cornea. Ophthalmology 2006; 113:2203-8. [PMID: 17157133].

32. Micali A, Pisani A, Puzzolo D, Nowińska A, Wylegala E, Teper S, Czajka E, Roszkowska AM, Orzechowska-Wylegala B, Aragona P. Macular corneal dystrophy: in vivo confocal and structural data. Ophthalmology 2014; 121:1164-73. [PMID: 24491640].

33. Saito T, Nishida K, Nakayama J, Akama TO, Fukuda MN, Watanabe K, Quantock AJ, Maeda N, Watanabe H, Tano Y. Sulfation patterns of keratan sulfate in different macular corneal dystrophy immunophenotypes using three different probes. Br J Ophthalmol 2008; 92:1434-6. doi:10.1136/bjo.2008.139527[PMID: 18815430].

34. Akhtar S, Alkatan HM, Kirat O, Khan AA, Almubrad T. Collagen Fibrils and Proteoglycans of Macular Dystrophy Cornea: Ultrastructure and 3D Transmission Electron Tomography. Microsc Microanal 2015; 21:666-79. [PMID: 25939479].

35. Nowinska AK, Wylegala E, Teper S, Wróblewska-Czajka E, Aragona P, Roszkowska AM, Micali A, Pisani A, Puzzolo D. Phenotype and genotype analysis in patients with macular corneal dystrophy. Br J Ophthalmol 2014; 98:1514-21. [PMID: 24926691].

Articles are provided courtesy of Emory University and The Abraham J. & Phyllis Katz Foundation. The print version of this article was created on 4 October 2024. This reflects all typographical corrections and errata to the article through that date. Details of any changes may be found in the online version of the article.